



Delft University of Technology

CryoSat ocean product quality status and future evolution

Bouffard, Jerome; Naeije, Marc; Banks, Christopher J.; Calafat, Francisco M.; Cipollini, Paolo; Snaith, Helen M.; Webb, Erica; Hall, Amanda; Mannan, Rubinder; Féménias, Pierre

DOI

[10.1016/j.asr.2017.11.043](https://doi.org/10.1016/j.asr.2017.11.043)

Publication date

2018

Document Version

Final published version

Published in

Advances in Space Research

Citation (APA)

Bouffard, J., Naeije, M., Banks, C. J., Calafat, F. M., Cipollini, P., Snaith, H. M., Webb, E., Hall, A., Mannan, R., Féménias, P., & Parrinello, T. (2018). CryoSat ocean product quality status and future evolution. *Advances in Space Research*, 62(6), 1549-1563. <https://doi.org/10.1016/j.asr.2017.11.043>

Important note

To cite this publication, please use the final published version (if applicable).

Please check the document version above.

Copyright

Other than for strictly personal use, it is not permitted to download, forward or distribute the text or part of it, without the consent of the author(s) and/or copyright holder(s), unless the work is under an open content license such as Creative Commons.

Takedown policy

Please contact us and provide details if you believe this document breaches copyrights.
We will remove access to the work immediately and investigate your claim.



Available online at www.sciencedirect.com

ScienceDirect

Advances in Space Research 62 (2018) 1549–1563

**ADVANCES IN
SPACE
RESEARCH**
(*a COSPAR publication*)
www.elsevier.com/locate/asr

CryoSat ocean product quality status and future evolution

Jerome Bouffard ^{a,*}, Marc Naeije ^b, Christopher J. Banks ^d, Francisco M. Calafat ^d, Paolo Cipollini ^c, Helen M. Snaith ^e, Erica Webb ^f, Amanda Hall ^f, Rubinder Mannan ^f, Pierre Féménias ^g, Tommaso Parrinello ^g

^a RHEA – System clo ESA – ESRIN, Earth Observation Directorate, 2 Via Galileo Galilei 2, 00044 Frascati, Italy

^b Space Engineering, Delft University of Technology, Delft, The Netherlands

^c National Oceanography Centre, European Way, Southampton SO14 3ZH, UK

^d National Oceanography Centre, Joseph Proudman Building 6, Brownlow Street, Liverpool L3 5DA, UK

^e British Oceanographic Data Centre, National Oceanography Centre, European Way, Southampton SO14 3ZH, UK

^f Telespazio VEGA UK Ltd., 350 Capability Green, Luton, Bedfordshire LU1 3LU, UK

^g ESA – ESRIN, Earth Observation Directorate, 2 Via Galileo Galilei 2, 00044 Frascati, Italy

Received 28 February 2017; received in revised form 27 November 2017; accepted 29 November 2017

Available online 7 December 2017

Abstract

The main objectives of this paper are to present the status of the CryoSat ocean products and to give an overview of all associated quality control and validation activities. Launched in 2010, the polar-orbiting European Space Agency's (ESA) CryoSat mission was primarily developed to measure changes in the thickness of polar sea ice and elevation of the ice sheets. Going beyond its ice-monitoring objective, CryoSat is also a valuable source of data for the oceanographic community. The satellite's radar altimeter can measure high-resolution geophysical parameters from the open ocean to the coast. To enable their full scientific and operational exploitation, the ocean products continuously evolve and need to be quality-controlled and thoroughly validated via science-oriented diagnostics based on multi-platform *in situ* data, models and other satellite missions. In support to ESA, the CryoSat ocean validation teams conduct this quality assessment for both the near real time and offline ocean products, both over short time scales (daily and monthly monitoring) and long-term stability (annual trends). Based on the outcomes from these quality analyses and feedback from scientific oceanographic community, ESA intends to upgrade the CryoSat Ocean processing chain for Autumn 2017.

© 2017 COSPAR. Published by Elsevier Ltd. All rights reserved.

Keywords: CryoSat; Satellite altimetry; Ocean; Quality assessment; Long-term stability; Ocean product evolution; Climate

1. Introduction

CryoSat-2 (hereafter CryoSat) is a 7-year radar altimetry mission, launched on 8 April 2010 with the primary objectives to monitor variations in the thickness of the Earth's marine ice cover and continental ice sheets ([Wingham et al., 2006](#)). The primary payload on-board CryoSat is the Synthetic Aperture Interferometric Radar

Altimeter (SIRAL), which has been monitoring the Earth's cryosphere with unprecedented accuracy and precision ([Parrinello et al., 2018](#); introduction of this CryoSat Special Issue). However, beyond the primary mission objectives, CryoSat also represents a valuable source of data for the oceanographic community. The quasi-geodetic orbit of CryoSat and the design of its altimeter are fundamentally different from the majority of existing ocean altimeters with the ability to reach polar regions and obtain higher-resolution data. These two specialties have opened the door for innovative data processing developments and have also

* Corresponding author.

E-mail address: Jerome.bouffard@esa.int (J. Bouffard).

contributed to improving the characterisation of the surface topography dynamics over the polar, coastal and open ocean domains.

The choice of the CryoSat orbit was initially the result of a trade-off between the desired high density of cross-over points over the Polar Regions and the need to sufficiently cover south Greenland (see Fig. 1). For this, the CryoSat orbit has a mean altitude of 717 km and a high inclination of 92°, allowing measurements at high latitudes (up to 88°). This orbit is non-sun-synchronous and the satellite drifts through all angles to the Sun in approximately 16 months. The repeat cycle for CryoSat orbit should be 369 days, corresponding to 5344 revolutions. However, the CryoSat orbit does not repeat exactly after each cycle, as is usually the case for ocean-oriented altimetry missions. CryoSat's ascending nodes are repeated from cycle to cycle within a few tens of meters in order to have equidistant ascending equator crossings in the reference ground track. The descending nodes are however no longer equidistant due to a residual rotation of the eccentricity vector, entailing fluctuations up to nearly 4 km from cycle to cycle. Despite this drifting geodetic orbit, which is not optimal for oceanographic applications, CryoSat has compensated for the loss of ENVISAT for operational oceanography and the characterisation of mesoscale dynamics (Labroue et al., 2012; Dibarbourre et al., 2011; Le Traon et al., 2015). CryoSat has also greatly contributed to enhancing the quality of the global mean sea surface (Andersen et al., 2015) and monitoring of the Arctic geostrophic circulation (Armitage et al., 2017), through the intensive sampling

of polar and altimetric inter-track areas that are not covered by conventional ocean-oriented missions.

SIRAL is the primary instrument on-board CryoSat and is considered the precursor for a new generation of altimeter systems, like those for the Sentinel-3 and Sentinel-6 ocean topography missions. The SIRAL instrument combines a conventional pulse-limited radar altimeter with synthetic aperture and interferometric signal processing (see Table 1). This single frequency Ku-band radar altimeter is capable of operating in three modes: Low Resolution Mode (LRM), Synthetic Aperture Radar (SAR) and SAR Interferometric (SARIn or SIN) burst modes.

Each mode was initially designed for optimal measurements over different surfaces. The measurement modes are operated on-board according to a geographical mode mask (see Fig. 1), which is updated regularly to allow for the changing extent of sea-ice and to track sea ice boundaries. Over the oceans and ice sheet interiors, CryoSat generally operates in LRM, similar to traditional pulse-limited radar altimeters. Over sea ice, SAR mode is used, whereby coherently transmitted echoes are combined via a delay-Doppler processing, reducing the illuminated surface area (Raney, 1998). SAR mode is mainly used to carry out high-resolution measurements of floating sea ice. CryoSat's most advanced mode is generally used around the margins of continental ice sheets and over mountain glaciers where topography is steep. Here, the altimeter performs SAR altimetry measurements and uses a second antenna as an interferometer to determine the across-track angle to the earliest radar returns. This SARIn mode provides the exact location of the surface being measured.

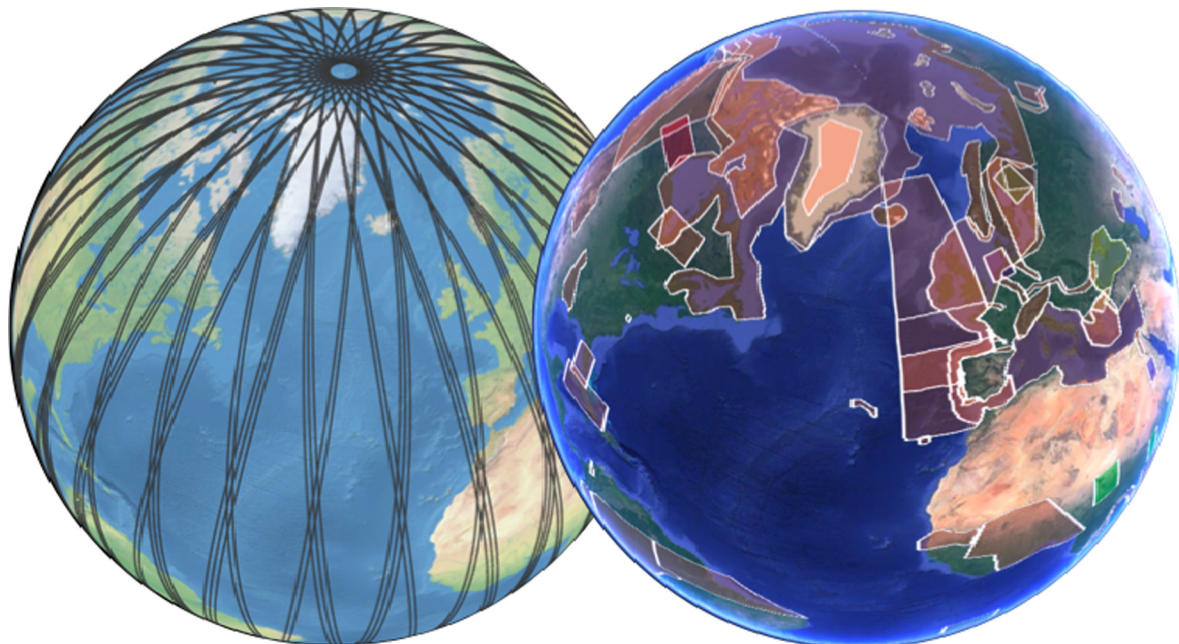


Fig. 1. (left) CryoSat ground track coverage from 01/10/17 to 05/10/17 (black lines) and (right) Geographical mask of acquisition according to operational mode (version 3.9, in place since 30 January 2017) More details on: https://earth.esa.int/web/guest/missions/esa-operational-eo-missions/cryosat/content/-asset_publisher/VeF6/content/geographical-mode-mask-7107.

Table 1
SIRAL instrument characteristics.

Radio frequency	13.575 GHz (single frequency Ku-band)
Pulse bandwidth	320 MHz (40 MHz for tracking only in SIN)
Pulse Repetition Frequency (PRF)	1.97 kHz in LRM, 18.181 kHz in SAR and in SIN
Burst mode PRF	N/A in LRM, 85.7 Hz in SAR, 21.4 Hz in SIN
Compressed pulse length	3.125 ns
Pulse duration	44.8 μ s
Timing	Regular PRF in LRM, burst mode in SAR and SIN
Samples in echo	128 in LRM and SAR, 512 in SIN
RF peak power	25 W
Antenna size	2 reflectors 1.2 m \times 1.1 m, side-by-side
Antenna beamwidth (3 dB)	1.06° (along-track) \times 1.1992° (across-track)
Antenna footprint	15 km
Range bin sample	0.2342 m for SAR/SIN, 0.4684 m for LRM
Data rate	60 kbit/s for LRM, 12 Mbit/s in SAR, 2 \times 12 Mbit/s in SIN
Instrument mass (with antennas)	90 kg redundant
Instrument power	149 W
Tracking cycle	47.17 ms (not a multiple of PRF)
Burst repetition	11.8 ms (not a multiple of PRF)
Antenna baseline length	1167.6 mm

The CryoSat geographical mode mask is however not static and regular updates are made by the European Space Agency (ESA), considering requests from the coastal altimetry and oceanographic community. A number of changes have been made over the past seven years in order to stimulate research and development activities (e.g. SARIn boxes over Cuba and Greece islands, SAR box over North East Atlantic), and to support the quality assessment of Sentinel-3 ocean topography data during the commissioning phase (e.g. SAR box over the Pacific). Although the primary mission objective of CryoSat is to observe the cryosphere, its measurements over the ocean are indeed of great value to the oceanographic and climate research communities, as testified by many contributions to the Ocean Surface Topography Science Team (OSTST) meetings (<http://www.aviso.altimetry.fr/en/user-corner/science-teams/ostst-swt-science-team.html>) and Coastal Altimetry Workshops (www.coastalt.eu/community).

Consequently, thanks to fruitful collaborations with the Centre National d'Études Spatiales (CNES) and the National Oceanic and Atmospheric Administration (NOAA), ESA has developed and implemented its own CryoSat Ocean Processor (COP), to operationally generate CryoSat products specifically designed for oceanographers. The COP includes up-to-date and ocean-oriented algorithms and corrections in order to bridge the gap between previous and future ocean missions as well as to contribute to a better knowledge of polar circulation. Since 2014, CryoSat data are processed simultaneously by both Ice and Ocean processors, generating a range of operational ocean products, with specific latencies, alongside the original ice products (see Fig. 2). The CryoSat Ice processors and the COP operate almost independently and follow two distinct processing baselines. The COP uses input Level 0 (L0) LRM and SAR data and generates Level 1B (L1B) and Level 2 (L2) products using Pseudo-Low Resolution Mode (PLRM) techniques over the SAR mode

patches of the global mask, by processing the pulse-limited echoes incoherently, as in the conventional LRM concept (Scharroo, 2014). These products are generated at two latencies: Intermediate Ocean Products (IOP) generated typically two to three days after acquisition for medium-range ocean forecasting (using the CNES Medium Orbit Ephemeris (MOE)); and Geophysical Ocean Products (GOP) generated typically 30 days after acquisition with consolidated orbits (using the CNES Precise Orbit Ephemeris (POE)) and corrections for longer-term, retrospective and climate studies. They complement the Near-Real Time (NRT) Fast Delivery Marine (FDM) products currently generated by the Ice processor (using the Doris Navigator Orbit).

The CryoSat ocean products (FDM, IOP and GOP) are routinely monitored for Quality Control (QC) by the ESA/ESRIN Sensor Performance, Products and Algorithms (SPPA) office with the support of the Instrument Data quality Evaluation and Analysis Service (IDEAS+). These basic QC activities include checking data availability and processing completeness, the usage of the correct Auxiliary Data Files and calibration files in processing; and checking that no error flags are raised in the data.

Alongside these activities, the ocean products are analysed in more detail at the UK National Oceanography Centre (NOC), within the framework of the CryoSat Ocean product Quality Control and Validation (CryOcean-QCV) project. This activity includes two complementary aspects: (i) global assessment and quality control of the data over the oceans; (ii) validation against *in situ* observations, other altimetry datasets and numerical models. The global assessment is conducted both daily (for FDM and IOP) and monthly (for FDM, IOP, and GOP) for the sea surface height anomaly (SSHA), significant wave height (SWH), radar backscattering coefficient (σ_0), wind speed, and mispointing parameters. The validation is performed

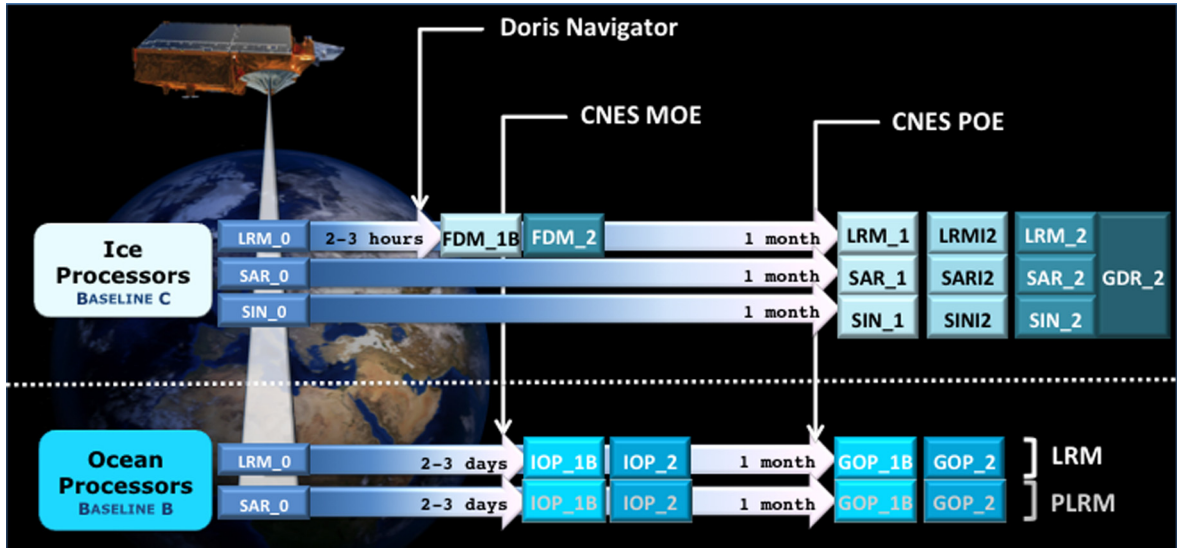


Fig. 2. Two independent CryoSat processors for ice and ocean applications (FDM: Fast Delivery Mode, LRM: Low Resolution Mode, PLRM: Pseudo-LRM, IOP: Intermediate Ocean Product, GOP: Geophysical Ocean Product). The suffixes _1, _1B, _2 and I2 refer respectively to Level-1 (Level-1B+ Full Bit Rate products), Level-1B, Level-2 and In-Depth Level-2 products. More details can be found at https://earth.esa.int/web/guest/-/products-overview-6975#_101_INSTANCE_VeF6_matmp.

monthly for the GOP SSHA, geostrophic velocity, SWH and wind speed. Results of the assessment and validation are extensively described in daily and monthly reports available on the ESA website (see Section 3) and have been recently published in Calafat et al. (2017).

In parallel, a complementary quality assessment of the GOP Level 2 data is performed by the Delft University of Technology (TU Delft), as a continuation of previous calibration and validation activities performed by Naeije et al. (2011) and Schrama et al. (2014, 2016). The main goal is long-term monitoring; evaluating the stability of the measurement system and identifying potential biases and drifts. This is achieved through cross-calibration with concurrent ocean altimeter data from Jason-2 (launched 20th June 2008) which is considered as the reference mission from the completion of its commissioning phase and until it moves to an interleaved orbit (September 2016). Independently, this is also addressed by comparing the GOP sea level anomaly with *in situ* data from a selected set of tide gauges. Since a good altimeter ocean product requires a very precise determination of the orbital height, the quality of CryoSat's precise orbit data from the Centre National d'Etudes Spatiales (CNES) is also assessed by independently generating precise orbits and cross-validating them (Schrama, 2017).

This paper provides an overview of the CryoSat ocean data quality status. After briefly presenting the COP baselines, the paper focuses on the activities and results associated with the ocean quality assessment, both from routine and long-term analysis. Finally, we discuss the forthcoming evolution of the processing chains and validation approaches to accommodate future releases of upgraded CryoSat ocean products. This paper is complementary to Bouffard et al. (2018) (this issue) focusing on the SIRAL

performance, stability and quality control and validation activities over the sea-ice and land-ice domains.

2. CryoSat ocean product characteristics

2.1. Content of the Level 2 ocean products

The CryoSat L2 ocean products mainly contain measurements of the sea surface height (SSH), the SWH and wind speed derived from the processing of the radar waveforms in both LRM and PLRM (over SAR patches). This is done by using the Ocean-3 or MLE-4 algorithm (Amarouche et al., 2004), where the measured waveform is fitted with a 4-parameter return power model, according to weighted Least Square Estimators derived from Maximum Likelihood Estimators (MLE). Fitting the raw waveforms with a waveform model (Brown, 1977) yields estimates of the location, amplitude and rising time of the waveform. The location or epoch is converted into the fundamental measure of range, which is then used to compute the SSH as detailed below. The amplitude of the waveform gives an estimate of the radar backscattering sigma₀, which is then converted into wind following Abdalla (2007). The waveform rise time (inversely proportional to the slope of the leading edge of the waveform) is directly linked to SWH in the Brown model.

The principal parameter generated by the COP is the SSH over a reference ellipsoid (WGS84 ellipsoid). SSH computation involves correcting the range for a series of propagation delays and geophysical effects and subtracting it from the orbit:

$$\text{SSH} = \text{altitude} - (\text{range} + \text{ssha_corrections}) \quad (1)$$

where `ssha_corrections` is a sum of all range and geophysical corrections, which are identified by the addends in the sum below and are also available as individual fields in the CryoSat ocean products:

$$\begin{aligned}
 \text{ssha_corrections} = & \text{ionospheric correction} \\
 & + \text{dry tropospheric correction} \\
 & + \text{wet tropospheric correction} \\
 & + \text{sea state bias} + \text{solid earth tide} \\
 & + \text{ocean loading tide} + \text{ocean tide} \\
 & + \text{long period ocean tide} \\
 & + \text{geocentric pole tide} \\
 & + \text{dynamic atmospheric correction} \\
 & + \text{inverse barometric correction}
 \end{aligned} \quad (2)$$

If a geoid model of sufficient accuracy is available, this can be subtracted from the corrected SSH to derive the dynamic topography of the ocean. However, more often the SSH is quality controlled, verified and used in the form of its anomaly (SSHA) with respect to a chosen

$$\text{Mean Sea Surface (MSS)} : \text{SSHA} = \text{SSH} - \text{MSS} \quad (3)$$

For a description of the ocean products, we refer the reader to the CryoSat Product Handbook: https://earth.esa.int/documents/10174/125272/CryoSat_Product_Handbook. Further details on the specific geophysical parameters and corrections analysed in routine quality control and validation activities, as well as in the long-term analysis of the CryoSat ocean products can be also found in Sections 3.1.1 and 3.2.1 respectively.

2.2. Ocean product processing baselines

The first CryoSat Ocean Processor (COP) became operational on 10/04/2014 and IOP and GOP for the period from 10/04/2014 to 22/02/2015 were generated with the COP Baseline-A. After this date, the COP was upgraded to Baseline-B with a new processing configuration and new Calibration 1 (Cal1) corrections. New Look-Up Table (LUT) corrections and CNES orbit model standard (GDR-E), required to align the ocean products with the operational Baseline-C ice products, were integrated on 01/04/2015. The Baseline-A ocean data were then definitively removed from the CryoSat dissemination server 6 months after the COP Baseline-B went in operation (see Fig. 3).

Within the framework of the COP evolution activities, 12 months of GOP data (July 2013–June 2014) were reprocessed with the updated Baseline-B GOP, for the purpose of internal testing and to define new algorithms in preparation for the future COP Baseline-C. IDEAS+ performed detailed validation of a 5-day Test Data Set (TDS) from each month of the campaign, including the verification of quality flags, parameter and correction values, as well as

auxiliary and calibration file usage within the products. Following the good validation results obtained (see Section 3.2), ESA decided to extend the Baseline-B reprocessing campaign to the full CryoSat GOP L1B and L2 dataset from November 2010 to March 2015 and to disseminate the data to ocean users awaiting the COP Baseline-C and subsequent reprocessing campaign planned for 2018 (Fig. 4). The full-reprocessed Baseline-B GOP dataset from November 2010 to March 2015 is accessible to registered users from the CryoSat dissemination server (<ftp://science-pds.cryosat.esa.int>).

This Baseline-B reprocessed dataset is of good quality but, due to operational constraints, shows a bias and a slight inconsistency affecting LRM parameters (not PLRM). As detailed in Section 3.2, these expected biases could be easily corrected. Before 22/02/2015, the LRM range can be corrected by applying a spatial and temporal constant value of +0.7203 m. Before and after 27/03/2015, the LRM backscatter coefficients show an average difference of ~0.37 dB, linked to the use of different Cal1 corrections (estimation of internal delay of the SIRAL through measuring the impulse response). This could cause a mean difference of ~+0.4 mm, ~2 mm and 1.1 m/s for the retrieved LRM sea state bias (SSB), SWH and wind speed respectively. These known issues are not critical for most oceanographic applications and will be fixed with the introduction of COP Baseline-C and associated reprocessing campaign (see Section 5).

In the meantime, the FDM (from the Baseline-C Ice processor) and the IOP and GOP (from the Baseline-B COP) continue to be distributed, regularly quality controlled and in-depth validated by ESA with the support of CryoSat mission partners from the TU Delft, the NOC and the IDEAS+ consortium.

3. Ocean product quality assessment

3.1. Routine quality control and scientific validation

3.1.1. Data and methods

IDEAS+ performs routine QC activities on all operational CryoSat products, which include checking L0 data availability; acquisition tracking and L0 echo errors; the product headers; the product formats and software versions; the Auxiliary Data File usage; the external correction error flags and the analysis of measurement parameters. IDEAS+ uses a number of different tools and software to perform their operational analyses. The CryoSat-2 Quality Control – Quality Analysis of Data from Atmospheric Sensors (C2QC-QUADAS) is an updated tool installed in April 2015 at the Payload Data Segment (PDS) and on local machines at Telespazio Vega UK. It is configured to monitor both operational and reprocessed ice and ocean data products, and to automatically generate daily and monthly QC reports, which form the basis of the IDEAS+ daily performance reports. The Quality Control for CryoSat (QCC) tool is installed at

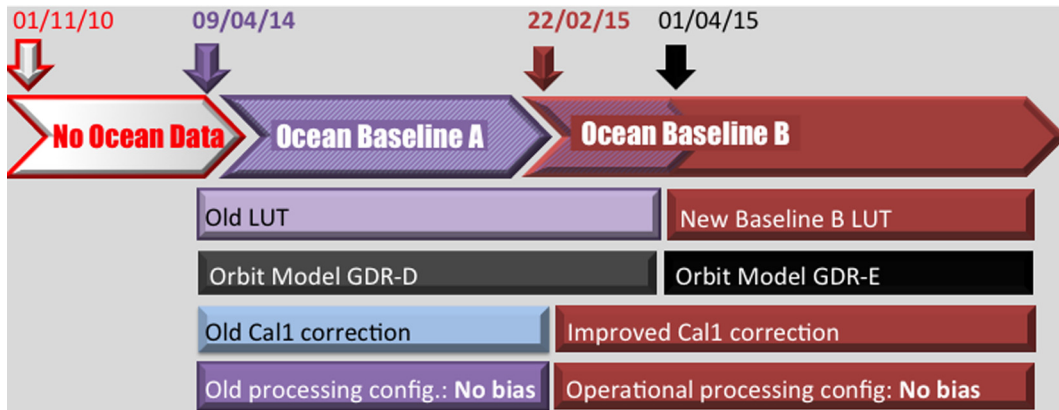


Fig. 3. GOP availability and characteristics. Situation before November 2016.

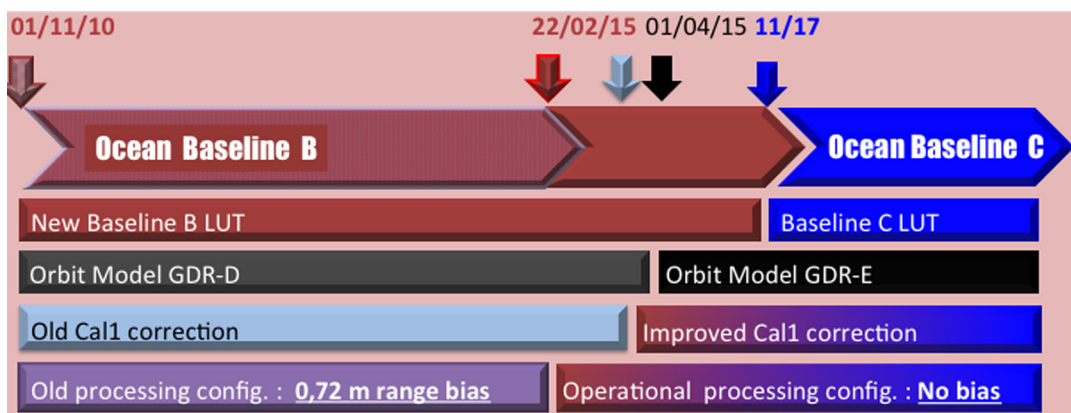


Fig. 4. GOP availability and characteristics. Situation on November 2017 (before the start of the COP Baseline-C processing campaign).

the PDS and is designed to perform a set of configurable checks on each product immediately after production. This information is checked and included in the IDEAS+ daily performance reports, which are uploaded daily to the ESA CryoSat webpage (<https://earth.esa.int/web/guest/missions/esa-operational-eo-missions/cryosat/daily-performance-reports>).

Complementary to the IDEAS+ activities, more scientific Quality Control and Validation (CryOcean-QCV) activities are performed by the NOC using a fully automated system. This system first downloads the necessary CryoSat and validation datasets, then generates relevant statistics and figures using all available data, then compiles a report incorporating relevant text and figures, and finally uploads the report to the ESA file servers. The system is automated by a series of scripts, developed and implemented at the NOC. The data download is scheduled to run twice daily, whilst other scripts run daily or monthly, depending on the report type.

As part of the assessment, all CryoSat ocean data are screened according to scientific quality criteria (in addition to the quality control flags provided within the product files), including the use of minimum and maximum thresholds for the range and geophysical corrections and for the

values of sigma0, SSHA, SWH and their corresponding 20 Hz standard deviations. The assessment is global in scope and includes coverage, completeness and data flow, global along-track analysis, crossover analysis, spectral statistics and derivation of error levels. Table 2 lists the models used to derive the various corrections, which in turn are used in the validation of the SSH and SSHA calculation in Baseline-B products, as described in (Eqs. (1)–(3)). Note that some models include more than one correction, for example the 2D Gravity Waves Model (MOG2D) is used to compute the Dynamic Atmosphere Correction (DAC), which includes the inverse barometric barometer correction. Another example is the ocean tide model, which includes also the loading tides and the long period tides. Such cases are highlighted in the table. The CNES-Collecte Localisation Satellites 11 (CNES-CLS 11) model is used as a reference MSS. It should be noted that the data products also contain alternative models for some of the variables, for example the Global Ocean Tide 4.8 (GOT4.8) tide model (Ray, 2013) is available as an alternative to Finite Element Solution 2014 (FES2014), and the Technical University of Denmark 10 (DTU10) MSS (Andersen and Knudsen, 2010) as an alternative to CNES-CLS11.

Table 2

Models used by the NOC for the various corrections in the COP Baseline-B.

Corrections	Measurement or Model	Notes
<i>Ionospheric (iono)</i>	Global Ionospheric Map (GIM) (Near-Real-Time) (Mannucci et al., 1998)	Bent model (Bent et al., 1975) where GIM not available
<i>Dry Tropospheric (dry_tropo)</i>	European Centre for Medium-Range Weather Forecasts (ECMWF)	Operational model at its highest spatial resolution ($1/8^\circ$), 6-h interval
<i>Wet Tropospheric (wet_tropo)</i>	ECMWF	Operational model at its highest spatial resolution ($1/8^\circ$), 6-h interval
<i>Sea State Bias (ssb)</i>	LRM/PLRM: CLS model (Tran, 2012)	
<i>Solid Earth Tide (solid_earth_tide)</i>	Cartwright-Taylor-Edden model (Cartwright and Taylor, 1971; Cartwright and Edden, 1973)	
<i>Ocean Tide (ocean_tide_sol1)</i>	GOT4.8 (Ray, 2013)	
<i>Ocean Tide (ocean_tide_sol2)</i>	FES2004 (Lyard et al., 2006)	
<i>Ocean Loading Tide (loading_tide_sol1)</i>	GOT4.8 (Ray, 2013)	Already included in ocean_tide_sol1
<i>Ocean Loading Tide (loading_tide_sol2)</i>	FES2004	Already included in ocean_tide_sol2
<i>Long Period Tide (long_period_tide)</i>	FES2004	Already included in ocean_tide_sol1 and ocean_tide_sol2
<i>Geocentric Pole Tide (pole_tide)</i>	Desai (2002)	
<i>Dynamic Atmospheric Correction (dynamic atmosphere)</i>	MOG2D (Carrère and Lyard, 2003)	Includes low frequency
<i>Inverse Barometric (inverse_barometric)</i>	ECMWF	Operational model at its highest spatial resolution ($1/8^\circ$), 6-h interval. Already included in MOG2D DAC

GOP SSHs are validated against tide gauge records from all around the world. The validation with tide gauge records includes both relative and absolute comparisons. The relative comparisons are between time series of sea level from tide gauges and GOP SSH anomalies; both referenced to an arbitrary zero level. The absolute validation is between absolute GOP SSHs and heights derived from tide gauge records, both ellipsoidal heights above the same reference ellipsoid, and is only possible at sites where there is a good levelling link between the tide gauge benchmark and a nearby Global Positioning System (GPS), i.e. the levelled height difference between the GPS station and the tide-gauge benchmark is known, and the distance between the GPS station and tide gauge is small. These sites include La Coruña, Spring Bay, Marseille, Ponta Delgada, Chichijima, Virginia Key, and Funafuti. The distance between the tide gauge and the GPS station is smaller than 2.6 km in all cases, and smaller than 5 m at four of the stations. Tide gauge records are obtained from the UK National Tide Gauge Network archives at the British Oceanographic Data Centre (BODC) (at 15-min resolution) and the University of Hawaii Sea Level Centre (UHSLC) (at 1-h resolution). Ellipsoidal heights were computed using GPS station data obtained from Système d'Observation du Niveau des Eaux Littorales (SONEL) (<http://www.sonel.org/>). All GPS heights are defined with respect to ITRF2008, in consistency with the sea surface heights from CryoSat. GOP SSH anomalies are also compared with Argo-derived steric heights over the global oceans. The set of Argo profiles were obtained from the EN4.1.1 data set made available by the Met Office Hadley Centre (<http://hadobs.metoffice.com/en4/>).

The GOP SWH is validated against both *in situ* hourly buoy data obtained from the National Data Buoy Centre (NDBC) and hourly modelled data from the WaveWatch III global wave model obtained from the Pacific Islands Ocean Observing System at the University of Hawaii. The Wavewatch III model provides hourly values of SWH over the global ocean at $1/2^\circ$ spatial resolution. The Wavewatch III model is a third-generation wave model developed at NOAA/National Centres for Environmental Prediction (NCEP), which solves the random phase spectral action density balance equation for wave-number direction spectra (Tolman, 2009). The comparison between CryoSat SWH and buoy data are restricted to buoys located in the open ocean no closer than 20 km to the coast.

Finally, as part of the validation activities, geostrophic velocities are derived from the GOP SSHA and compared High Frequency (HF) radar surface velocities from four stations around the Australian coast (Bonney Coast, Rottnest Shelf, South Australia Gulfs, and Turquoise Coast) from the Australian Ocean Data Network (<https://portal.aodn.org.au/>), as well as against geostrophic velocities from the Ocean Surface Current Analyses Real time (OSCAR) (<http://www.oscar.noaa.gov>). The HF radar data are provided on a fine regular grid with a 1-h temporal resolution, whereas the OSCAR data are provided on a $1/3$ -degree grid with a 5-day temporal resolution.

3.1.2. Main results

The full results of the CryOcean-QCV are disseminated in daily and monthly reports that are available on the ESA SPPA web server (<https://earth.esa.int/web/sppa/mission->

performance/esa-missions/cryosat/quality-control-reports/ocean-product-quality-reports). A comprehensive summary of the results has been recently published in Calafat et al. (2017). We provide here some examples to illustrate the level of analysis and validation.

The first example concerns the FDM data products, which are made available as soon as possible after acquisition, normally within 3 h. This short latency from acquisition to dissemination is essential to enable NRT applications, and is assessed within the CryOcean-QCV reports. For example, Fig. 5 illustrates the distribution of FDM data delivery latency for September 2016 and is typical of many of the monthly plots. The majority of data were delivered within 2–3 h of the middle time of the measurements within the files.

Our second example concerns the SWH, which is an important measurement from satellite altimetry for wave climate studies, the study of extreme events and the validation of wave models. As shown in Calafat et al. (2017), there is a good agreement between SWH from CryoSat and that obtained from the WWIII data. A typical example of the agreement between WWIII and GOP can be seen in the similar distributions of SWH in Fig. 6.

Two examples are used to illustrate the quality of the SSH measurements from CryoSat and the derived geostrophic velocities. Geostrophic currents are calculated as a function of latitude from GOP data within two study regions, one region in the Atlantic Ocean (20°N – 40°N , 315°E – 325°E) and another in the Pacific Ocean (20°N – 40°N , 220°E – 230°E). The velocities are calculated using the optimal difference operator by Powell and Leben (2004) and are compared with the equivalent data from OSCAR in Fig. 7 for September 2016. With a few obvious exceptions in the Atlantic at lower latitudes and at 33°N (Fig. 7, top), the OSCAR and GOP derived velocities agree in terms of magnitude and direction.

The monthly reports produced for CryOcean-QCV include a selection of randomly selected Argo floats for

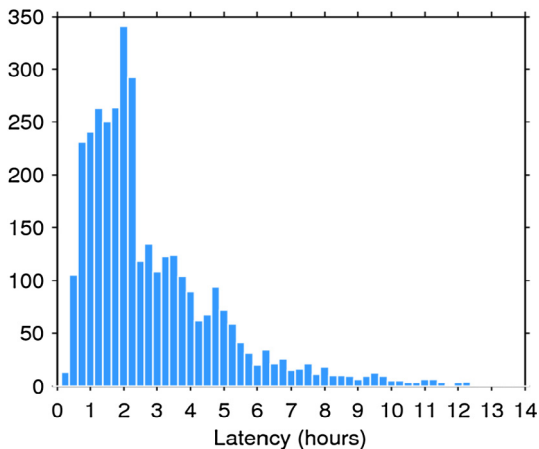


Fig. 5. Histogram of the FDM data delivery latency for September 2016. The y-axis shows the number of files that are made available with a delay of x-hours with respect to the mean time of the records stored in the file.

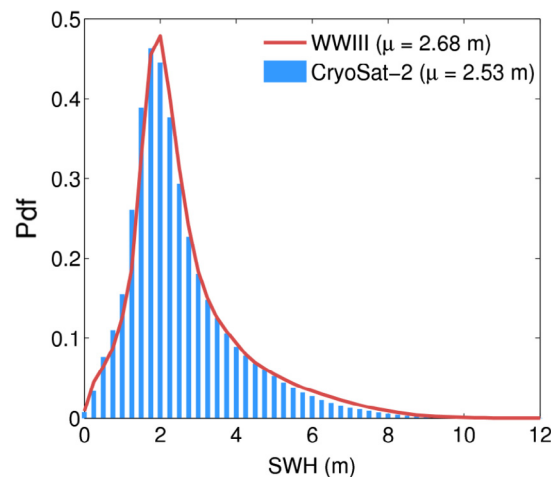


Fig. 6. Histograms (normalised to have a total area of 1) of the GOP SWH (blue bars) and the SWH from the Wavewatch III model (red line) for September 2016. (For interpretation of the references to colour in this figure legend, the reader is referred to the web version of this article.)

which the steric height anomalies are calculated over the top 1000 m. These anomalies are then compared with the SSHA from GOP data. A sample plot is shown in Fig. 8 (top), and the movement of the given float, in this case ID 5,904,174, is given in Fig. 8 (bottom). The GOP SSAs are calculated by interpolating the ground track data from a 1° by 1° grid, every 10 days in order to match the 10-day cycle of an Argo float.

In addition to the CryOcean-QCV analysis, which mainly focuses on short-term variability (daily, monthly) and seasonal time scales, complementary analyses are conducted to assess the long-term performance and stability of the GOP and to identify potential drift and bias.

3.2. Long-term analysis and data quality stability

3.2.1. Data and methods

To assess the long-term quality of the CryoSat GOP in comparison with other reference ocean altimetry missions, geophysical parameters such as SSHA, SWH, backscatter (σ_0), and wind speed referenced to 10 m height (U_{10}) are monitored and cross-calibrated. This is done using the Radar Altimeter Database System (RADS) <http://rads.tudelft.nl/rads/rads.shtml> (Scharroo et al., 2016). RADS is a coordinated effort between EUMETSAT, NOAA, and Delft University of Technology (TU Delft), and constitutes an internationally appreciated validated, calibrated and consistent altimeter data set, comprising over 20 years of sea level products, to help both expert and entry-level users in science and education to apply altimeter information in their own investigations. Since multiple users are involved in examining the data and the regular updates to the database, RADS is one of the most accurate and complete databases of satellite altimeter data to date, and therefore is most suited for referencing and cross-calibrating the CryoSat GOP data. The 1 Hz L2 CryoSat

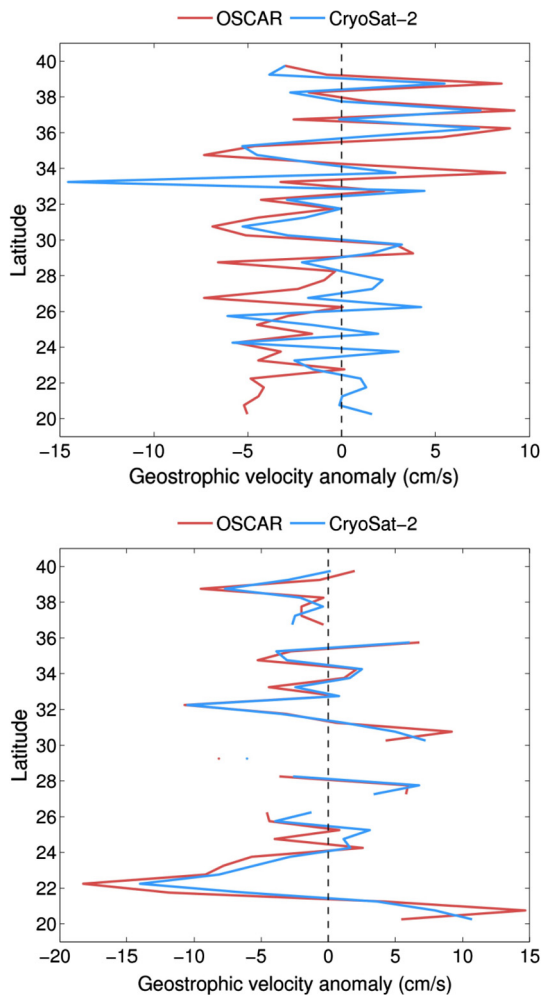


Fig. 7. Comparison of the GOP geostrophic velocity anomalies with geostrophic velocity anomalies from the Ocean Surface Current Analyses – Real time (OSCAR) for September 2016 in the Atlantic (top, 20°N–40°N, 315°E–325°E) and Pacific (bottom, 20°N–40°N, 220°E–230°E) boxes as a function of latitude (i.e., for each latitude the geostrophic velocities have been averaged over the longitudes within the box). GOP geostrophic velocities have been computed using the optimal difference operator by Powell and Leben (2004).

data that are available in RADS, have been constructed from re-tracking L1B LRM data and wherever the instrument is in SAR mode, using the Full Bit Rate (FBR) data to reduce SAR to PLRM (Scharroo et al., 2013; Scharroo, 2014).

The operational Baseline-B GOP L2 data that are analysed here, are distilled from the ESA's ftp server and cover the period from April 2015 to July 2016 and the reprocessed data from February 2012 to April 2015. First, they are stored in subcycles, according to the RADS cycle definition for CryoSat, with the following sequence: 4 times (29 + 29 + 27 days) plus 29 days makes 369 days, which is the theoretical repeat cycle for CryoSat. The data are also archived in RADS format, choosing the appropriate data fields to facilitate the cross-calibration with Jason-2, for example by decomposing the total tide into ocean tide

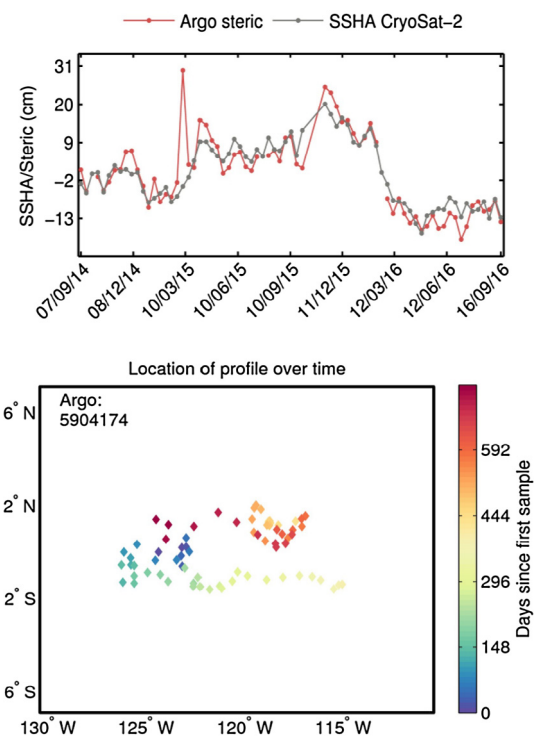


Fig. 8. Comparison of the GOP SSHA and the steric height anomaly (referred to 1000 m) for one particular Argo float (top). The location of the Argo float over time (bottom).

and load tide. The DAC is considered as the total inverse barometric correction (the static low frequency part and the high frequency part of the tidal and atmospheric signal). The square root of the off-nadir pointing is taken, and the orbital altitude, geoid, and mean sea surface are referenced to the TOPEX reference ellipsoid ($a = 6378136.3$ m, $1/f = 298.257$). The remaining GOP data fields are untreated and copied directly to the corresponding RADS fields. SSHA are calculated and Jason-2 data are chosen for comparison and crossover analyses for the same period (Jason-2 cycles 132–294). Table 3 summarises which data fields from the GOP are entered into RADS and describes the treatment of the data. The data are not altered in order to ensure that they remain as close as possible to the original GOP product.

SSHA are subsequently created by taking the difference between orbit and range and subtracting all corrections and lastly subtracting a MSS model, as described in (Eqs. (1)–(3)). For the corrections and models that have multiple options, it is necessary to choose the same correction as is used in the altimeter data you want to compare (Jason-2 in this case).

To validate the ocean sea level data with tide gauge observations the revised local reference data are extracted from the Permanent Service for Mean Sea Level (PSMSL) database at NOC/ Natural Environment Research Council (NERC) (Holgate et al., 2013; PSMSL, 2016). An effort is made to ensure that before comparison both altimetry and tide gauge data have matching physical content by using

Table 3

The RADS format and the treatment of the L2 GOP data when entered into the RADS. The GOP field numbers are taken from the IOP and GOP product format Specification (ACS/CLS, 2013).

RADS item	Item no.	RADS comment	GOP field	GOP to RADS treatment
<i>Time</i>	101	UTC since 1985-01-01 00:00:00 [s]	1	$d * 86,400 + s + \mu s / 1d6 + sec00^a$
<i>Lat</i>	201	Latitude [degrees north]	7	Untreated
<i>Lon</i>	301	Longitude [degrees east]	9	Untreated
<i>Alt</i>	425	Orbital altitude [m]	11	WGS84 to TOPEX ref. ^b
<i>Alt rate</i>	501	Orbital altitude rate [m/s]	13	Untreated
<i>Range</i>	601	Instrument corrected altimeter range [m]	21	Untreated
<i>Dry tropo</i>	701	Dry tropospheric correction [m]	36	Untreated
<i>Wet tropo</i>	802	Wet tropospheric correction [m]	37	Untreated
<i>Iono</i>	906	GIM ionospheric correction [m]	40	Untreated
<i>Inv bar</i>	1002	High-frequency inverse barometric correction [m]	39–38	Untreated ^c
<i>Inv bar</i>	1004	Total inverse barometric correction [m]	39	Untreated
<i>Tide solid</i>	1101	Solid earth tide [m]	84	Untreated
<i>Tide ocean</i>	1213	FES2004 ocean tide [m]	79–83	Total ocean tide – load tide
<i>Tide ocean</i>	1219	GOT4.8 ocean tide [m]	78–82	Total ocean tide – load tide
<i>Tide load</i>	1313	FES2004 load tide [m]	83	Untreated
<i>Tide load</i>	1319	GOT4.8 load tide [m]	82	Untreated
<i>Tide pole</i>	1401	Pole tide [m]	85	Untreated
<i>SSB</i>	1502	CLS sea state bias [m]	41	Untreated
<i>Geoid</i>	1610	EGM2008 height [m]	74	WGS84 to TOPEX ref.
<i>MSS</i>	1614	DTU10 mean sea surface [m]	73	WGS84 to TOPEX ref.
<i>MSS</i>	1615	CNESCLS11 mean sea surface [m]	72	WGS84 to TOPEX ref.
<i>SWH</i>	1701	Significant wave height [m]	44	Untreated
<i>Sig0</i>	1801	Backscatter coefficient [dB]	51	Untreated
<i>Wind speed</i>	1901	Altimeter wind speed [m/s]	87	Untreated
<i>Range rms</i>	2002	Std dev of range (20 Hz) [m]	23	Untreated
<i>Range num</i>	2101	Number averaged 20 Hz ranges [count]	24	Untreated
<i>Topo</i>	2206	MACESS ocean depth/elevation [m]	75	Untreated
<i>Peakiness</i>	2401	Peakiness [-]	16	Untreated
<i>Flags</i>	2601	Engineering flags [-]	90&14	RADS flags (bits 24,511)
<i>SWH rms</i>	2802	Std dev of SWH (20 Hz) [m]	47	Untreated
<i>Sig0 rms</i>	2902	Std dev of sig0 (20 Hz) [dB]	53	Untreated
<i>Off nadir</i>	3001	Waveform off-nadir pointing [degrees]	62	Take square root
<i>Ref frame</i>	3801	Reference frame offset [m]	—	— ^d

^a sec00 = 473,299,200 s offset to get time relative to 1 January 1985 instead of 1 January 2000.

^b RADS employs the TOPEX ellipsoid definition: $a = 6378136.3$ m, $1/f = 298.257$.

^c Correction used for tide gauges analyses

^d Unknown a priori and therefore not applied initially.

monthly averaged tide gauge data, thereby filtering out most of the residual high frequency tidal and atmospheric signals. The total ocean tide correction and the high frequency part of the atmospheric signal are applied to the altimeter data, therefore keeping the low frequency static inverse barometer in the altimeter data. Next, monthly altimeter grid solutions are constructed, combining data per month (~ 1 subcycle), and spatially Gaussian distance weighting gridding with a $\sigma = 0.5^\circ$, a horizon of 3σ and grid-spacing of 0.25° , and used to produce SSHA time series at the tide gauge station locations. All the available, matching tide gauge and altimeter data were used, and an integer number of consecutive years were analysed to enable the estimation of drift over the years 2013, 2014, and 2015. The tide gauge data available for the chosen time span were selected, reducing the dataset from 1468 gauges to 491. For the next step in aligning the altimetry based SSHA to the tide gauge measurements; only stations with a correlation higher than 0.7 and a standard deviation of $\sigma < 0.1$ m were considered. A common bias in the tide

gauges, which are referenced to local mean sea level and not to the TOPEX reference ellipsoid, was also removed. The 72-cm offset present in the GOP data prior to February 2015 (see Section 2.2) was also removed, and stations with data gaps were excluded. This reduced the dataset further to 213 gauges, which were used for the following statistical analyses.

3.2.2. Main results

Within the framework of long-term GOP analysis, orbit crossover analysis was performed on the L2 GOP altimeter data, spanning February 2012 to July 2016. Crossovers were analysed between CryoSat and Jason-2 passes (dual satellite crossovers) and between ascending and descending passes from CryoSat and Jason-2 separately (single satellite crossovers), with a maximum crossover time difference of 15 days; a narrower time interval would leave very few CryoSat crossovers spread non-uniformly over the globe.

The mean crossover differences between CryoSat and Jason-2 passes provide the biases between CryoSat and

the calibrated Jason-2. As a reference for both satellites the CNES/CLS11 mean sea surface and the GOT4.8 ocean tide and ocean load corrections are applied. Comparing CryoSat with Jason-2 (CryoSat minus Jason-2) basically gives a range bias with respect to Jason-2. However, for Jason-2, a calibrated range bias with respect to the TOPEX reference ellipsoid is already applied and therefore the mean crossover difference between CryoSat and Jason-2 gives a calibrated range bias for CryoSat. From the statistics, an overall range bias change is observed in February 2015, where the SSHA cycle averages change from minus 72 cm (prior to February 2015) to approximately zero (after February 2015) due to configuration changes in the Baseline-B COP baseline (see Section 2). As a result of this change, it was decided to investigate a 1-year period before this date (period 1: 15 June 2013 to 15 June 2014) and a 1-year period after (period 2: 5 June 2015 to 15 June 2016). Table 4 provides the matching overall dual-crossover statistics. Crossovers have been edited to discard SSHA crossover values greater than two times the standard deviation, in order to incorporate only crossovers that are not strongly affected by ocean mesoscale variability. As stated before, the standard criterion $t < 2$ days would eliminate too many crossovers.

SWH, sigma0 and wind speed have also been included in the crossover analyses. Since the two points evaluated in a crossover analysis can be relatively far apart in time for the time scales at which these parameters can change, it can still be seen that taking the mean of the crossover differences would average out those difference (mean values are close to zero). They do constitute a means of quality checking the parameters. Therefore, it can be concluded that the CryoSat GOP is of the same quality as the CryoSat RADS product and also very close to the calibrated Jason-2. The only striking difference is in the range and the sigma0 biases. This difference should be studied in more detail because the SSB also has a dependency on sigma0.

Finally, Table 5 provides for the same data products and data fields the satellite single crossovers (for period 2: 5 June 2015 to 15 June 2016). When edited exactly in the same manner, the SSHA crossover RMS is slightly higher for CryoSat GOP than for CryoSat RADS and Jason-2. We conclude that the GOP product is of similar quality as both CryoSat RADS and Jason-2 RADS. The latter has lower crossover RMS because of its geographically limited coverage up to 66°N and 66°S.

There are two ways to estimate the timing bias, either from crossover minimisation or from the dependency of along-track residuals with the satellite range rate; both give

similar results. The envelope of timing biases from crossovers (with a maximum crossover standard deviation multiplied by two and a maximum time gap of 15 days) has been computed for the CryoSat GOP covering the period from February 2012 to July 2016. The overall average timing bias is 0.1 ms, Fig. 9 shows the daily estimated values (green), along with the mean crossover difference (red) and RMS (blue). The regression lines suggest a very steady timing bias, and also a stable crossover RMS at around 5 cm. If we exclude the main occurrence of the 72-cm offset in February 2015 and perform a fit to the SSHA crossover mean RMS prior to and after that date, the drift in both cases is smaller than 0.5 mm/year, indicating a very good stability comparable with the general uncertainty in sea level trend estimates. This conclusion of course assumes that the calibrated reference mission Jason-2 is not drifting. Any similar drifts in one or more of the corrections used would not be revealed by this cross calibration.

After applying the 72-cm bias change (subtracting a 72 cm bias) the comparison is conducted with the 213 selected tide gauges. The result is a mean correlation of $R = 0.85$, a mean standard deviation of $\sigma = 5.6$ cm, and a mean tilt of the difference of -0.5 mm/year ($\text{SSHA} - \text{tide gauge}$), which is comparable with the number found previously for the stability of the range. It is known that certain tide gauges may have problems if they are located on sediment and not bedrock or if they suffer from unknown vertical tectonic motions. However, the screening method adopted should remove most tide gauges affected by these problems. Fig. 10 plots the locations of the 213 tide gauge stations used in this study (grey crosses). The blue crosses represent the ten best comparisons when sorted by correlation and the red crosses represent the worst two comparisons when sorted by standard deviation.

Fig. 11 shows the three best solutions in terms of correlation and the worst solution in terms of standard deviation, where the correlation (C_o), the standard deviation (S_t), the bias (B_i), and the trend difference (S_l) are given (refer to Fig. 10 for the position of corresponding tide gauges).

In summary, the long-term analysis of CryoSat GOP shows a steady timing error of 0.1 ms, and a stable range bias of 6.7 cm with no marked drift with respect to calibrated Jason-2 (TOPEX reference ellipsoid and reference mission). These results obtained over the ocean are perfectly consistent with the results deduced from external calibrations performed on the ground at the Svalbard transponder, which also show very stable values (see Bouffard et al., 2018; this issue). When validated against 213 selected PSMSL tide

Table 4

Dual crossover mean and standard deviation from CryoSat and Jason-2 orbit crossovers for SSHA, SWH, σ^0 , and wind speed.

June 2013 until June 2014				June 2015 until June 2016			
SSHA [m]	SWH [m]	sigma0 [dB]	Wind speed [m/s]	SSHA [m]	SWH [m]	sigma0 [dB]	Wind speed [m/s]
Mean	-0.787	-0.011	-0.780	1.890	-0.067	-0.009	1.155
RMS	0.043	1.202	1.806	4.233	0.047	1.253	1.796

Table 5

Single crossover statistics for CryoSat GOP data, for CryoSat RADS data and Jason-2 RADS data (period 2: June 2015 until June 2016).

	SSHA [m]		SWH [m/s]		sigma0 [dB]		Wind speed [m/s]	
	Mean	RMS	Mean	RMS	Mean	RMS	Mean	RMS
CryoSat GOP	0.001	0.063	-0.003	1.259	0.023	2.256	-0.063	4.898
CryoSat RADS	0.005	0.056	-0.035	1.286	0.049	1.995	-0.139	3.996
Jason-2 RADS	0.000	0.040	-0.005	1.235	-0.003	1.650	0.009	3.953

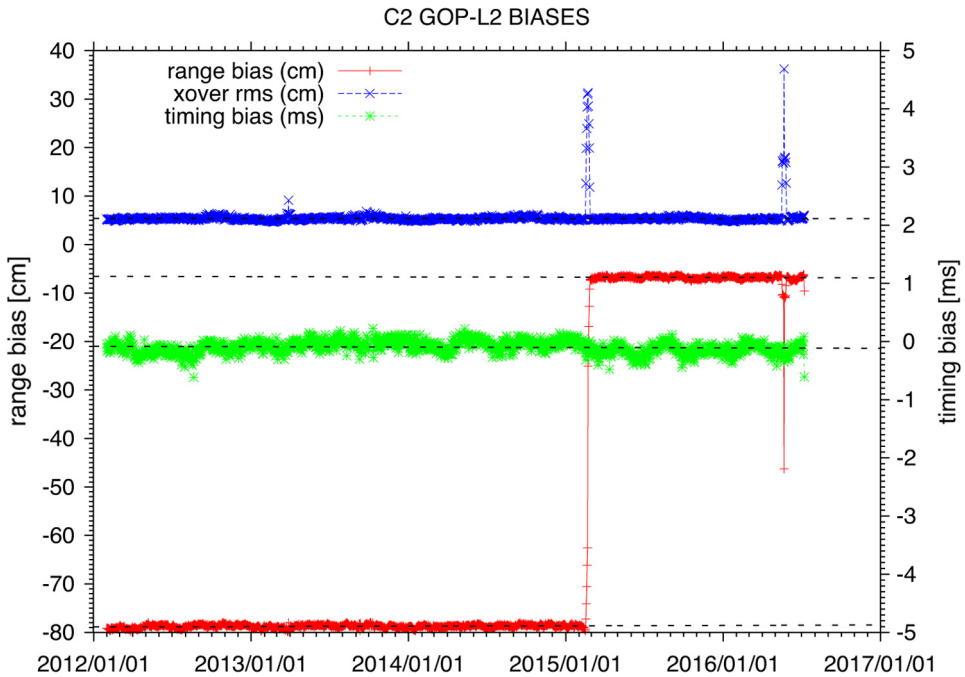


Fig. 9. Range bias (red) and timing bias (green) for CryoSat GOP cycles 24–81 (February 2012 until July 2016) along with the crossover standard deviation (blue). (For interpretation of the references to colour in this figure legend, the reader is referred to the web version of this article.)

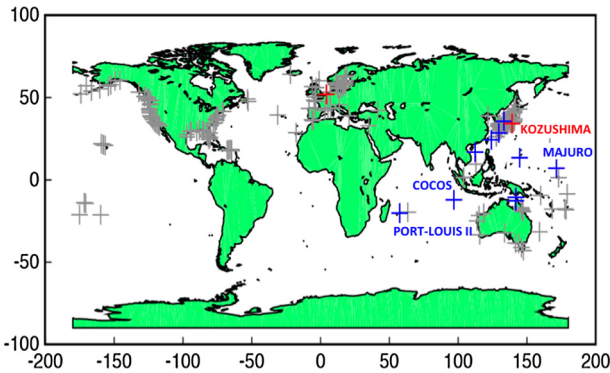


Fig. 10. Locations of the 213 PSMSL tide gauge station used in this study (grey). The 10 best solutions sorted by correlation (blue), and the 2 worst solutions sorted by standard deviation (red). (For interpretation of the references to colour in this figure legend, the reader is referred to the web version of this article.)

gauges, covering the period 2013–2015, the altimeter data have a correlation $R = 0.85$, a mean standard deviation $\sigma = 5.61$ cm, and a drift of -0.54 mm/year, again showing very stable measurements and no marked drift in the reference frame. Considering that TU Delft's orbit solutions

and laser residuals RMS are 0.4 mm/s and 1.27 cm, respectively and that they match the CNES POE (used in GOP) to within 1.5 cm radially, without showing any drift (Schrama et al., 2016; Schrama, 2018), the final conclusion is that the CryoSat GOP Baseline-B are comparable with the reference missions. Complementary analyses on reprocessed and upgraded GOP datasets (Baseline-C, see Section 4) are planned for 2018, in order to extend our results over a larger period and therefore confirm that the CryoSat ocean products would represent a valuable addition to long-term climate studies.

4. Brief overview of CryoSat ocean processing evolutions

ESA are continually working to improve the quality and scientific value of the CryoSat ocean products, by implementing improvements to the processing chains. Work is currently underway to test and implement the latest version processors, the COP Baseline-C. The Baseline-C upgrade concerns both the L1B and L2 processing chains and is expected to bring significant improvements to the quality of L1B and L2 products relative to the previous Baseline-B products. The new processors will generate ocean

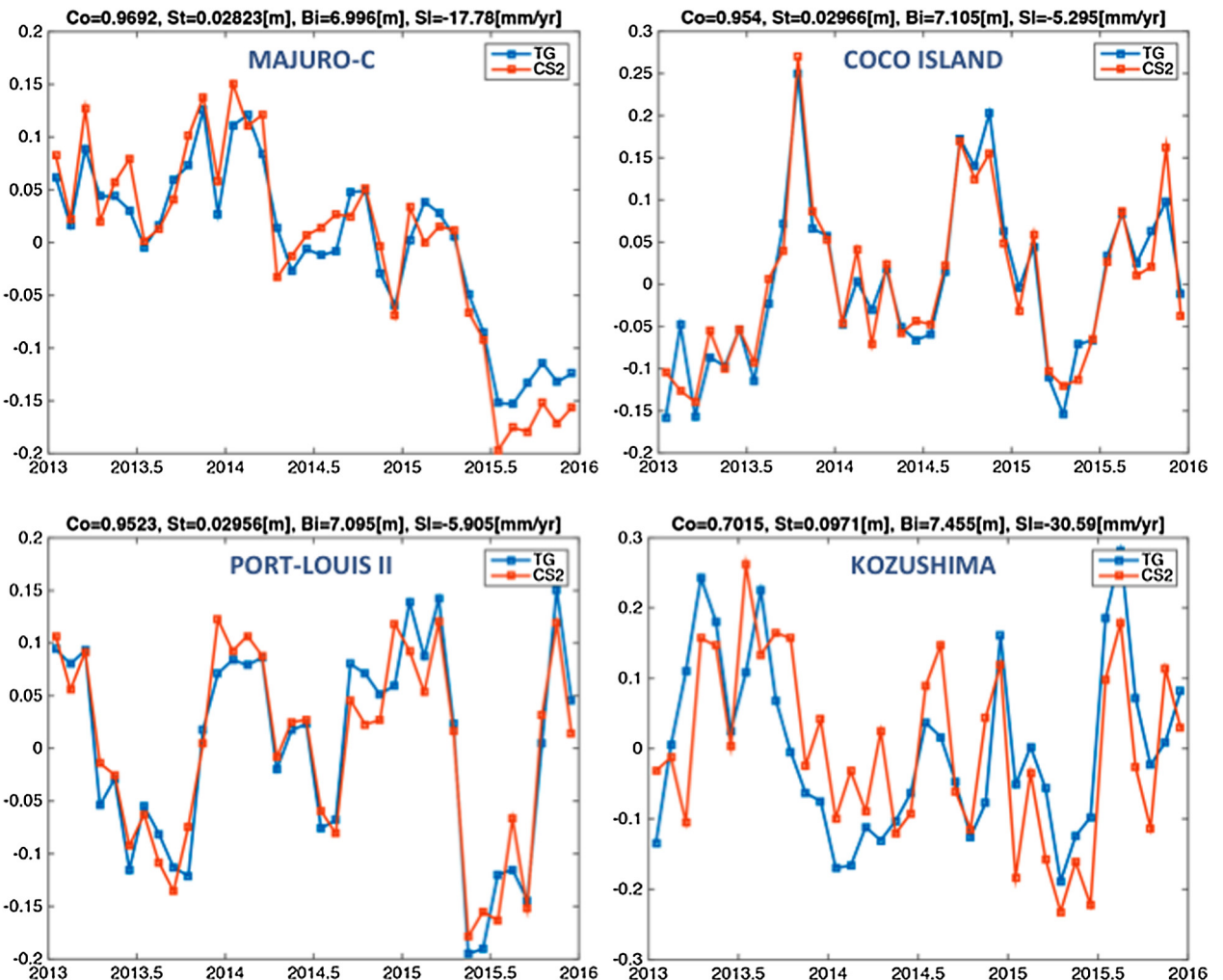


Fig. 11. Sea level data comparisons between PSMSL tide gauges (in blue) and CryoSat GOP (red). Locations of the tide gauge stations are reported on Fig. 10. The top two graphs and the bottom left graph show the three best results in terms of correlation (>0.95) and the bottom right graph shows the worst result in terms of standard deviation (≤ 10 cm). The graphs are each annotated with the correlation (Co), the standard deviation (St), the bias (Bi), and the trend difference (SI). (For interpretation of the references to colour in this figure legend, the reader is referred to the web version of this article.)

products for all data acquisition modes (LRM, SAR and SARIn), therefore providing complete data coverage for ocean users. The upgrade will add innovative algorithms to the ocean chains and refine some of the already implemented ones, and will add a number of new parameters and corrections to the products. Some of the expected evolutions are briefly described below. Routine distribution of the COP Baseline-C is starting in November 2017 (see Fig. 4).

4.1. New NetCDF and Pole-2-Pole ocean product format

In order to ensure the homogeneity with other altimetry missions and to maximise the uptake and use of CryoSat data by scientific users, ESA are currently upgrading the existing processing chains in order to distribute all CryoSat products in NetCDF format compliant with the Climate and Forecast Convention (<http://cfconventions.org>). NetCDF is considered to be more user-friendly than the Baseline-B COP Earth Explorer format, with data stored in a way to allow efficient subsetting. Interfaces to NetCDF

are based on the C library and are available in numerous languages (e.g. Matlab, IDL, Python, Octave), therefore enabling a wide range of software applications to read NetCDF files. Moreover, the Baseline-C COP will generate new L2 Pole-to-Pole (P2P) products for IOP and GOP. Two P2P products will be generated per orbit, combining successive products spanning between the North and South poles into multi-mode concatenated products.

4.2. New near real time ocean products

The COP architecture was initially designed so that it could be easily adapted to generate L1B and L2 products in NRT with an approximate latency of 3 h from data acquisition. In particular, the COP is already able to use the Doppler Orbitography and Radiopositioning Integrated by Satellite (DORIS) Navigator Orbit (Jaynes et al., 2015). Nevertheless, the current Baseline-B COP configuration requires some adaptations to generate NRT Ocean Products (NOP). Numerous evolutions will be

implemented to significantly improve the quality of the NOP with respect to the current FDM products generated by the Ice processor, such as the integration of full SAR delay-Doppler processing (see Section 4.2) and the addition of new ad-hoc corrections. As a result, the NOP is intended to replace the FDM products in mid-2018.

4.3. Full ocean delay-Doppler processing

ESA's SAR Altimetry MMode Studies and Applications (SAMOSA) retracker algorithm (Cotton et al., 2016) is being implemented and tested within the Baseline-C COP L2 processor. For this, the SAMOSA retracked SAR and SARIn waveforms are generated using new processors, which build on the Ice processor heritage but are correctly reconfigured for ocean applications. The SAMOSA retracker computes the 20 Hz epoch, amplitude, SWH and wind speed for SAR and SARIn (without using phase information). The 20 Hz altimeter range is then derived from the computed epoch and from the retracker range. The backscatter coefficient is derived from the computed amplitude and a scaling factor derived from the orbits and Automatic Gain Control (AGC) values. 1 Hz altimeter range, SWH and backscatter coefficients are also computed, simply by averaging the 20 Hz parameters. The SAMOSA derived 1 Hz and 20 Hz parameters are generated together with the PLRM parameters using the MLE-4 ocean retracker not only for SAR (as in COP Baseline-B) but also for SARIn patches. Therefore, the format of the L2 NOP, IOP and GOP products will be updated to include all these new fields.

4.4. New range and geophysical corrections

The Baseline-C COP products will include several new range and geophysical corrections, such as improved ocean and loading tidal corrections from the recent FES2014 and GOT4.10 (Zawadzki et al., 2016; Carrière et al., 2016; <https://datastore.cls.fr/catalogues/fes2014-tide-model/>) as well as the updated MSS from CNES (MSS_CNES_CLS15) and DTU (DTU MSS15). Since CryoSat does not carry an on-board microwave radiometer, one of the major COP upgrades concerns the inclusion of an improved wet tropospheric correction. The algorithm developed by the University of Porto, in the scope of the ESA CryoSat Plus for Ocean (CP4O) project, combines external wet path delay data from multiple sources by space-time objective analysis. More details on the approach can be found in Fernandes and Lazáro (2016).

5. Conclusions and perspectives

The quality control and validation activities performed by ESA with the support of the NOC, TU Delft and IDEAS+ demonstrate that the CryoSat ocean products compare very well with *in situ* measurements and model outputs and, in spite of the short analysed periods, do

not show any significant drift over time. The results confirm that the ocean products are comparable with reference ocean-oriented altimetry missions (e.g. Jason-2) and are perfectly suited for oceanographic applications.

The crossover analyses of GOP already revealed a very stable monitoring system capable of contributing to the Global Climate Observing System (GCOS) Essential Climate Variables (ECVs). ESA will continue to track possible biases, drifts and jumps in the data, and try to identify the potential causes and implement improved corrections. Another exercise will be to investigate the transitions from SAR to LRM and vice versa. Suggestions for improving sigma0 and wind speed could lead to reduced crossover RMS together with a tailored SSB correction. Concerning the tide gauge comparisons; the analyses will be extended to include inter-comparisons with Jason-3 data and updated CryoSat RADS data.

The quality control and validation tools are currently being upgraded to accommodate the upcoming processor upgrades to COP Baseline-C, as described in Bouffard (2016) and Bouffard et al. (2018) (this issue). The tools will be adapted to ingest the new L1B and L2 products in NetCDF format, including the new NOP and GOP and IOP P2P products from the ocean processor. In terms of product content the main changes concern the addition of native SAR/SARIn data over the relevant regions in the geographical mode mask, and a number of new parameters including updated geophysical corrections. These changes are expected to further improve the quality of the CryoSat ocean products and further promote their application to a broad range of oceanographic and climate studies.

References

- Abdalla, S., 2007. Ku-band radar altimeter surface wind speed algorithm. Mar. Geod. 35, 276–298. <https://doi.org/10.1080/01490419.2012.718676>.
- ACS, CLS, (2013). IOP & GOP Product Format Specification, Issue 1.4, C2-RS-ACS-ESL-5213. Available at: <https://earth.esa.int/documents/10174/125273/CryoSat_IOP_GOP_Product_Format_Specification_FMT>.
- Amarouche, L., Thibaut, P., Zanife, O.Z., Vincent, P., Steunou, N., 2004. Improving the Jason-1 ground retracking to better account for attitude effects. Mar. Geod., Part 2 27 (1–2), 171–197, Special Issue on Jason-1 Calibration/Validation.
- Andersen, O. B., Knudsen, P., 2010. The DTU10 mean sea surface and mean dynamic topography – Improvements in the Arctic and coastal zone. In: Presentation at the Ocean Surface Topography Science Team Meeting, October 2010, Lisbon, Portugal.
- Andersen, O.B., Knudsen, P., Stenseng, L., 2015. The DTU13 MSS (mean sea surface) and MDT (mean dynamic topography) from 20 years of satellite altimetry. In: Jin, S., Barzaghi, R. (Eds.), IGFS 2014. International Association of Geodesy Symposia. Springer, Berlin, pp. 111–121. https://doi.org/10.1007/1345_2015_182.
- Armitage, T.W., Bacon, S., Ridout, A.L., Petty, A.A., Wolbach, S., Tsamados, M., 2017. Arctic Ocean surface geostrophic circulation 2003–2014. Cryosphere 11, 1767–1780. <https://doi.org/10.5194/tc-11-1767-2017>.
- Bent, R.B., Llewellyn, S.K., Nesterczuk, G., Schmid, P.E., 1975. The development of a highly-successful worldwide empirical ionospheric model and its use in certain aspects of space communications and worldwide total electron content investigations. In: Goodman, J.M.

- (Ed.), 2016. Effect of the ionosphere on space systems and communications. Naval Research Laboratory, Washington, pp. 13–28.
- Bouffard, J., Féménias, P., Parrinello, T., Bojkov, B., 2016. CryoSat Mission: data quality status and next product evolutions. In: Presentation at the 4th CryoSat User Workshop, 9–13 May 2016, Prague, Czech Republic.
- Bouffard, J., Webb, E., Scagliola, M., Garcia-Mondéjar, A., Baker, S., Brockley, D., Gaudelli, J., Muir, A., Hall, A., Mannan, R., Roca, M., Fornari, M., Féménias, P., Parrinello, T., 2018. CryoSat instrument performance and ice product quality status. *Adv. Space Res.* 62 (6), 1526–1548.
- Brown, G., 1977. The average impulse response of a rough surface and its applications. *IEEE Trans. Antenn. Propag.* 25, 67–74. <https://doi.org/10.1109/TAP.1977.1141536>.
- Calafat, F.M., Cipollini, P., Bouffard, J., Snaith, H., Féménias, P., 2017. Evaluation of new CryoSat products over the ocean. *Remote Sens. Environ.* 191, 131–144. <https://doi.org/10.1016/j.rse.2017.01.009>.
- Carrère, L., Lyard, F., 2003. Modeling the barotropic response of the global ocean to atmospheric wind and pressure forcing – comparisons with observations. *Geophys. Res. Lett.* 30 (6), 1275. <https://doi.org/10.1029/2002GL016473>.
- Carrère, L., Lyard, F., Cancet, M., Guillot, A., Picot, N., 2016. FES 2014, a new tidal mode – Validation results and perspectives for improvements. In: Presentation at the ESA Living Planet Conference, 9–13 May 2016, ESA, Prague, Czech Republic.
- Cartwright, D.E., Edden, A.C., 1973. Corrected tables of tidal harmonics. *Geophys. J. Int.* 33 (3), 253–264. <https://doi.org/10.1111/j.1365-246X.1973.tb03420.x>.
- Cartwright, D.E., Tayler, R.J., 1971. New computations of the tide-generating potential. *Geophys. J. Int.* 23 (1), 45–73. <https://doi.org/10.1111/j.1365-246X.1971.tb01803.x>.
- Cotton, P.D., Andersen, O.B., Stenseng, L., Boy, F., Cancet, M., Cipollini, P., Gommenginger, C., Dinardo, S., Egido, A., Fernandes, M.J., Nilo-Garcia, P., Moreau, T., Naeije, M., Scharroo, R., Lucas, B., Benveniste, J., 2016. Improved Oceanographic Measurements with CryoSat SAR Altimetry: Results and Roadmap from ESA CryoSat Plus for Oceans Project. In: Proceeding of the ESA Living Planet Symposium, 9–13 May 2016, ESA Special Publication SP-740 (CD-ROM), Prague, Czech Republic. <http://www.satoc.eu/projects/CP4O/docs/0519cotton%20_CP4Oroadmap.pdf>.
- Desai, S.D., 2002. Observing the pole tide with satellite altimetry. *J. Geophys. Res.: Ocean* 107 (C11), 3186. <https://doi.org/10.1029/2001JC001224>.
- Dibarboire, G., Renaudie, C., Pujol, M.I., Labroue, S., Picot, N., 2011. A demonstration of the potential of CryoSat-2 to contribute to mesoscale observation. *Adv. Space Res.* 50 (8), 1046–1061. <https://doi.org/10.1016/j.asr.2011.07.002>.
- Fernandes, M.J., Lázaro, C., 2016. GPD+ wet tropospheric corrections for CryoSat-2 and GFO altimetry missions. *Remote Sens.* 8 (10), 851. <https://doi.org/10.3390/rs8100851>.
- Holgate, S.J., Matthews, A., Woodworth, P.L., Rickards, L.J., Tamisiea, M.E., Bradshaw, E., Foden, P.R., Gordon, K.M., Jevrejeva, S., Pugh, J., 2013. New data systems and products at the permanent service for mean sea level. *J. Coastal Res.* 29 (3), 493–504. <https://doi.org/10.2112/JCOASTRES-D-12-00175.1>.
- Jayles, C., Chaveau, J.-P., Auriol, A., 2015. DORIS/DIODE: real-time orbit determination performance on board SARAL/AltiKa. *Mar. Geod.* 38 (S1), 233–248. <https://doi.org/10.1080/01490419.2015.1015695>.
- Labroue, S., Boy, F., Picot, N., Urvoy, M., Ablain, M., 2012. First quality assessment of the Cryosat-2 altimetric system over ocean. *Adv. Space Res.* 50 (8), 1030–1045. <https://doi.org/10.1016/j.asr.2011.11.018>.
- Le Traon, P.-Y., Antoine, D., Bentamy, A., Bonekamp, H., Breivik, L.A., Chapron, B., Corlett, G., Dibarboire, G., DiGiocomo, P., Donlon, C., Faugère, Y., Font, J., Girard-Ardhuin, F., Gohin, F., Johannessen, J.A., Kamachi, M., Lagerloef, G., Lambin, J., Larnicol, G., Le Borgne, P., Leuliette, E., Lindstrom, E., Martin, M.J., Maturi, E., Miller, L., Mingsen, L., Morrow, R., Reul, N., Rio, M.H., Roquet, H., Santoleri, R., Wilkin, J., 2015. Use of satellite observations for operational oceanography: recent achievements and future prospects. *J. Oper. Oceanogr.* 8 (Supp. 1), s12–s27. <https://doi.org/10.1080/1755876X.2015.1022050>.
- Lyard, F., Lefèvre, F., Letellier, T., Francis, O., 2006. Modelling the global ocean tides: a modern insight from FES2004. *Ocean Dynam.* 56, 394–415.
- Mannucci, A.J., Wilson, B.D., Yuan, D.N., Ho, C.H., Lindqwister, U.J., Runge, T.F., 1998. A global mapping technique for GPS-derived ionospheric total electron content measurements. *Radio Sci.* 33 (3), 565–582. <https://doi.org/10.1029/97RS02707>.
- Naeije, M., Schrama, E., Scharroo, R., 2011. Calibration and validation of CryoSat-2 low resolution mode data. In: Proceedings of the CryoSat Validation Workshop, 1–3 February 2011, ESA Special Publication SP-693 (CD ROM).
- Parrinello, T., Shepherd, A., Bouffard, J., Badessi, S., Casal, T., Fornari M., Maestroni, E., Scagliola, M., 2018. CryoSat: ESA's ice mission – Eight years in space. *Adv. Space Res.* 62 (6), 1178–1190.
- Powell, B.S., Leben, R.R., 2004. An optimal filter for geostrophic mesoscale currents from along-track satellite altimetry. *J. Atmos. Oceanic Technol.* 21 (10), 1633–1642. [https://doi.org/10.1175/1520-0426\(2004\)021<1633:AOFFGM>2.0.CO;2](https://doi.org/10.1175/1520-0426(2004)021<1633:AOFFGM>2.0.CO;2).
- PSMSL, 2016. Permanent Service for Mean Sea Level “Obtaining Tide Gauge Data”. Available at: <<http://www.psmsl.org/data/obtaining/>>.
- Raney, R.K., 1998. The delay/doppler radar altimeter. *IEEE Trans. Geosci. Remote Sens.* 36 (5), 1578–1588. <https://doi.org/10.1109/36.718861>.
- Ray, R.D., 2013. Precise comparisons of bottom-pressure and altimetric ocean tides. *J. Geophys. Res.* 118, 4570–4584.
- Scharroo, R., 2014. RADS RDSAR Algorithm Theoretical Basis Document. Version 0.3, CP4O Project Report.
- Scharroo, R., Leuliette, E., Naeije, M., Martin-Puig, C., Pires, N., 2016. RADS Version 4: An Efficient Way to Analyse the Multi-Mission Altimeter Database. In: Proceedings of the ESA Living Planet Symposium, 9–13 May 2016, ESA Special Publication SP-740 (CD-ROM), Prague, Czech Republic.
- Scharroo, R., Smith, W.H.F., Leuliette, E., Lilibridge, J., 2013. CryoSat-2: The other ocean altimeter. In: Presentation at the ESA Living Planet Symposium, 9–13 September, 2013, Edinburgh, Scotland.
- Schrama, E., 2018. Precision orbit determination performance for CryoSat-2 ISSN 0273-1177. *Adv. Space Res.* 61 (1), 235–247.
- Schrama, E., Naeije, M., Visser, P., 2016. CryoSat Precise Orbit Determination and SIRAL Ocean Data Validation. Version 3.0, Progress Report, ESRIN contract 4000112740. Delft University of Technology, Space Engineering.
- Schrama, E., Naeije, M., Visser, P., Shum, C.-K., 2014. CryoSat Precise Orbit Determination and Indirect Calibration of SIRAL. ESA contract 18196/04/NL/GS via CCN-3, Delft University of Technology, Space Engineering.
- Tolman, H.L., 2009. User manual and system documentation of WAVEWATCH III. Version 3.14, NOAA/NWS/NCEP/MMAB Technical Note 276.
- Tran, N., Philipps, S., Poisson, J.-C., Urien, S., Bronner, E., Picot, N., 2012. Impact of GDR-D standards on SSB corrections. OSTST, 22–29 September, 2012 Venice, Italy. <https://www.aviso.altimetry.fr/fileadmin/documents/OSTST/2012/oral/02_friday_28/01_instr_processing_I/01_IP1_Tran.pdf>.
- Wingham, D.J., Francis, C.R., Baker, S., Bouzinac, C., Brockley, D., Cullen, R., de Chateau-Thierry, P., Laxon, S.W., Mallow, U., Mavrocodos, C., Phalippou, L., Ratier, G., Rey, L., Rostan, F., Viau, P., Wallis, D.W., 2006. CryoSat: a mission to determine the fluctuations in Earth's land and marine ice fields. *Adv. Space Res.* 37 (4), 841–871. <https://doi.org/10.1016/j.asr.2005.07.027>.
- Zawadzki, L., Ablain, M., Carrère, L., Ray, R.D., Zelensky, N.P., Lyard, F., Guillot, A., Picot, N., 2016. Reduction of the 59-day error signal in the Mean Sea Level derived from TOPEX/Poseidon, Jason-1 and Jason-2 data with the latest FES and GOT ocean tide models. *Ocean Sci. Discuss.* <https://doi.org/10.5194/os-2016-19>.